Dynamic Phasor Modeling of the Single-Phase MMC under Modulation PSC-PWM

Glendy A. Catzin-Contreras, *Member, IEEE*, Gerardo Escobar, *Senior Member, IEEE*, Andres A. Valdez-Fernandez, *Senior Member, IEEE*, and Manuel J. Lopez-Sanchez

***Abstract*—This paper develops a model, based on the dynamic phasor approach, for the single-phase modular multilevel converter (MMC). The switching sequences for the MMC are generated by the phase-shifted carrier-based pulse-width modulation (PSC-PWM) scheme. The modeling process begins with the MMC state space model, from which the DC and the fundamental complex Fourier coefficients, called dynamic phasors, are extracted for both the original state variables and the switching functions. All capacitor voltages per phase are considered separately in the developed dynamic phasor-based model (DPhM) for the MMC, which contrast with the usual definition of variables based on the sum and difference of the capacitor voltages per arm. The developed MMC DPhM is able to reproduce the steady-state waveforms of all original state variables, including the ripple amplitude, as compared to the results obtained from the switched MMC. Furthermore, both the switched MMC under the PSC-PWM and the derived DPhM MMC show that all capacitors voltages converge to the same steady-state average value without adding an external balance controller, but only due to the natural balancing action of the PSC-PWM scheme, despite arbitrary initial conditions in such voltages.**

Link to graphical and video abstracts, and to code:
https://latamt.ieeer9.org/index.php/transactions/article/view/9305

***Index Terms*—Dynamic phasor, modeling, modular multilevel converter, phase-shifted carrier-based pulse-width modulation.**

I. Introduction

THE MODULAR multilevel converter (MMC), proposed in [1], is a topology that has received great attention from the scientific community in the last decade. Research works on MMC topologies have addressed issues such as their modulation [2], modeling [3]–[6], and control [7]–[11].

Either to improve simulation times or to aid in the controller design process, most of the models proposed for the MMC are based on averaging techniques [8]–[10], which generally consider the sum and difference of currents and voltages per arm in the MMC. This may represent a modeling drawback when there is an interest in the behavior at cell level. Moreover, averaged models are the starting point to develop other kind of models [11], such as those based on dynamic phasors (DPh), which are suitable for electromagnetic transient (EMT) simulations [4] or stability analysis [3], [5], [6]. Roughly speaking, DPhs are time-varying Fourier series coefficients that can model the fundamental component and the higher harmonics in a given system [12]. DPh-based modeling was introduced in [13] as a generalized averaging method. In particular, a dynamic phasor-based model (DPhM) is of great interest in the analysis of circuits involving periodically switched devices [3], [14].

A first DPhM for the MMC was reported in [3], which was intended for the analysis of the small signal stability. Other DPhMs used for small signal stability analysis of the MMC were developed in [5] and [6]. Yet another DPhM for the MMC was obtained in [4] with the purpose of carrying out EMT simulations. The modeling process based on DPhs in these works starts by obtaining the averaged model of the MMC in terms of sums and differences of the currents and voltages on the MMC arms. Then, the DPhs properties (to be reviewed later in this work) are applied to the averaged model to get the model of the MMC expressed in terms of the dynamic phasors, that is, a DPhM. In the DPhMs for the MMC, reported in [3]–[6], the state variables are described using sums and differences of the original variables. Similarly, switching (or insertion) signals' functions, are also expressed in terms of sums and differences of the original switching signals given at arm levels. Therefore, DPhs for switching signals at individual capacitor levels were not considered in those works.

Based on the DPhs approach, the present paper aims to develop and evaluate a model for the single-phase MMC that considers the original state variables of the converter, i.e., neither sums nor differences of the arm quantities are used in the modeling process [10], as commonly encountered in averaged techniques and also in the works using the DPhs approach. In fact, the proposed model considers DPhs for switching signals of every capacitor on the MMC, allowing to observe the MMC behavior at the cell level. Regarding the modulation stage, the PSC-PWM scheme has been selected for the generation of the switching sequences. This modulation scheme has reported a natural capacitor voltage balancing benefit [10], [15], [16]. To achieve this paper's objective, as an initial step, the mathematical model of the MMC is developed considering the original electrical variables. Then, the model is transformed by considering, as the new variables, the DC and the fundamental phasor components of the state variables and

The associate editor coordinating the review of this manuscript and approving it for publication was Suélia Fleury (*Corresponding author: Andres Alejandro Valdez-Fernandez*).

G. A. Catzin-Contreras is with the Universidad Politecnica de Yucatan, Ucu, 97357, Mexico (e-mail: ganyali@ieee.org).

G. Escobar is with the School of Engineering and Sciences, Tecnologico de Monterrey, Monterrey, 64849, Mexico (e-mail: gerardo.escobar@tec.mx).

Andres Alejandro Valdez-Fernandez is with the School of Sciences, Universidad Autonoma de San Luis Potosi, San Luis Potosi, 78295, Mexico (e-mail: andres.valdez@ieee.org)

M. J. Lopez-Sanchez is with the Universidad Autonoma de Yucatan, Mexico (e-mail: manuel.lopez@correo.uady.mx).

switching signals. For this, the methodology presented in [17] is adapted to the MMC topology to obtain its generalized averaging model, which is able to reproduce both the average and the ripple response of the state variables.

Thus, the developed model is able to reproduce the waveforms of the state variables in the original MMC, including their ripple amplitude. As an illustrative example, a detailed procedure to obtain the DPhM of a single-phase MMC with six cells on its phase is included. However, the modeling presented here can be easily extended to the case of an arbitrary number of cells on the single-phase MMC. The responses of the developed model are compared against the results of a switched MMC under the PSC-PWM scheme. Moreover, it is shown that the natural balancing performance, observed in the switched MMC under the PSC-PWM scheme, is also reproduced by the derived DPhM of the MMC. That is, independently of the initial conditions on the capacitor voltages, all capacitors converge to the same steady-state average value without adding an explicit balancing controller, but only due to the natural balancing action of the PSC-PWM scheme. This feature is known in the literature as a natural balancing mechanism [15], [16], [18].

Summarizing, the main contributions of the proposed DPhM with respect to previous works are described as follows:

- **(1)** A DPhM of the MMC topology considering every single capacitor voltage in the modeling process, instead of variables based on the sum and difference of the capacitor voltages on the arms. In this way, every cell voltage behavior can be observed.
- **(2)** A detailed procedure to obtain the DPhM of a single-phase MMC with six cells on its phase is provided.
- **(3)** Through the results obtained from the proposed DPhM and from the switched MMC, it is observed that the developed DPhM represents the steady-state waveforms of all state variables in the MMC, including their corresponding ripple amplitudes.
- **(4)** The DPhM reproduces the natural balancing of capacitor voltages observed in a real MMC operation under the PSC-PWM scheme.

The DPhM may be of great help in the design of an MMC, as the model's fast simulation allows to evaluate how the currents and voltages respond before specific values of parameters like the switching frequency, capacitances and inductances.

The rest of the paper is organized as follows: Section II presents the mathematical model of a single-phase MMC and the description of the PSC-PWM scheme. Section III shows the fundamentals of the DPh-based modeling technique. Based on the theory exposed in Section III, a DPhM of the MMC is developed in Section IV. Section V presents the simulation results of the developed DPhM and the real-time simulation of the switched MMC operating with the PSC-PWM scheme. Finally, Section VI presents the concluding remarks.

II. Description of the MMC and the PSC-PWM

A. MMC

Fig. 1 shows a single-phase MMC with a load impedance Z_0 connected at its output to model different types of load.

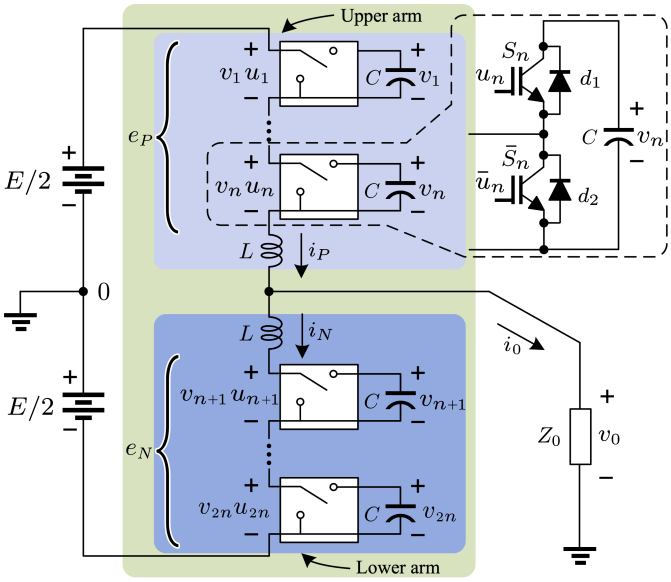

Fig. 1. Topology of the single-phase MMC of $2n{+}1$ levels.

This topology comprises two arms, namely, the upper and lower arms. Each arm comprises a series connection of n half-bridges, referred to as cells or submodules, plus an inductor. Each cell is composed of a pair of complementary IGBTs (with corresponding free-wheeling diodes) and a capacitor. The four possible current paths for the i-th cell of the MMC are shown in Fig. 2. Depending on which switch is in the ON state, the capacitor may be inserted or bypassed from the associated arm. That is, if the upper switch S_i is ON, the capacitor is inserted to the arm. This holds true independently of the direction of the current, i.e., if the current is flowing out from the terminal marked as positive, then the IGBT conducts (Fig. 2a); otherwise, if the current flow is reversed, diode d_1 conducts (Fig. 2b). However, if the switch $\bar{S}_i$ is ON, then the capacitor is bypassed (Figs. 2c and 2d); consequently, the voltage at the cell terminals is zero, irrespective of the current flow.

The mathematical model of the MMC depicted in Fig. 1, which is built with an arbitrary number n of cells on each arm, is described by

$$\frac{d}{dt}i_P = \frac{1}{L}\left(\frac{E}{2} - v_0 - e_P\right), \tag{1}$$

$$\frac{d}{dt}i_N = \frac{1}{L}\left(\frac{E}{2} + v_0 - e_N\right), \tag{2}$$

$$\frac{d}{dt}v_i = \frac{1}{C}i_P u_i, \quad \forall i \in \{1,\ldots,n\}, \tag{3}$$

$$\frac{d}{dt}v_i = \frac{1}{C}i_N u_i, \quad \forall i \in \{n+1,\ldots,2n\}, \tag{4}$$

where L is the arm inductance value; i_P and i_N represent the upper and lower arm currents, respectively; E is the DC-link voltage value; v_0 is the AC voltage; $e_P \triangleq \sum_{i=1}^{n} v_i u_i$ and $e_N \triangleq \sum_{i=n+1}^{2n} v_i u_i$ are the total inserted voltage in the upper and lower arms, respectively. The number of attainable levels in the output voltage depends on the modulation scheme used in the MMC, and it can be up to $2n{+}1$ levels. Finally, v_i is the

voltage of the i-th capacitor ($i \in 1, \ldots, 2n$), $u_i \in \{0, 1\}$ is the i-th switching signal ($i \in 1, \ldots, 2n$), and C is the capacitance.

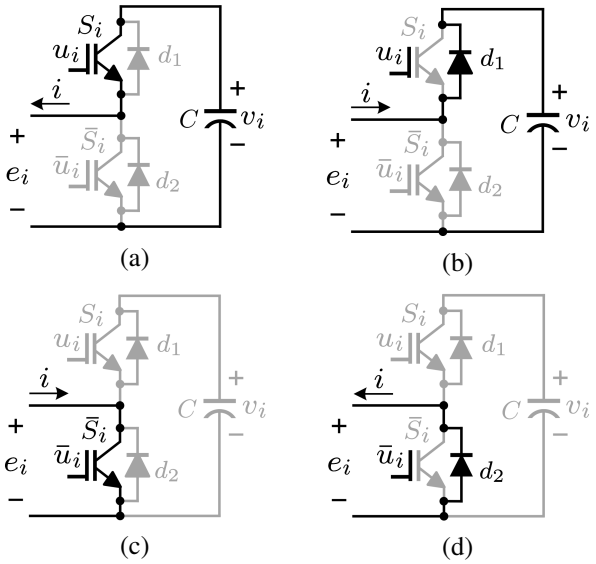

Fig. 2. Different current paths for the i-th cell ($i \in 1, \ldots, 2n$) of the MMC showing whether the capacitor is (**(a)** and **(b)**) inserted or (**(c)** and **(d)**) bypassed.

B. PSC-PWM

For a single-phase MMC, the PSC-PWM scheme considers two normalized sinusoidal references given by

$$D_P = 0.5\left(1 - m_a \sin\left(2\pi f_0 t\right)\right), \tag{5}$$

$$D_N = 0.5\left(1 + m_a \sin\left(2\pi f_0 t\right)\right), \tag{6}$$

where m_a is the modulation index and must be within the interval $0 \leq m_a \leq 1$ to avoid overmodulation, D_P and D_N are the modulating signals for the cells in the upper and lower arms, respectively, f_0 is the frequency of the modulating signals, and t denotes the time.

Regarding the carrier signals, the PSC-PWM requires as many triangular carrier waveforms (with frequency f_c) as the number of cells in the converter. The normalized amplitude of the carrier signals is in the range $[0, 1]$, whereas their i-th phase angle ϕ_i can be obtained using

$$\phi_i = \frac{2\pi}{n}(i-1) + \varphi, \qquad \forall i \in \{1, \ldots, n\}, \tag{7}$$

$$\phi_i = \frac{2\pi}{n}\left(i - (n+1)\right), \quad \forall i \in \{n+1, \ldots, 2n\}, \tag{8}$$

where $i \in \{1, \ldots, 2n\}$ represents the cell number in the MMC phase, ϕ_i is the i-th carrier phase angle on each cell, and φ is the phase-shift between the carriers of the upper and lower arms, which is selected as follows [19]

$$\varphi = 0\,, \quad n \quad \text{odd}, \tag{9}$$

$$\varphi = \frac{\pi}{n}, \quad n \quad \text{even}, \tag{10}$$

leading to a voltage signal of $2n{+}1$ levels at the converter's output. In this way, when n is odd, the set of carrier signals is the same in both arms.

III. The DPh-based Modeling Technique

In the DPh-based modeling technique, a time domain signal $x(t)$ on the interval $[t-T, t]$ can be expressed by the following complex Fourier series:

$$x(t) = \sum_{k=-\infty}^{\infty} \langle x \rangle_k(t) e^{jk\omega_c t}, \tag{11}$$

where $\omega_c = 2\pi/T$ is the angular switching frequency with T the converter's switching period; j is the imaginary unit, and $\langle x \rangle_k(t)$ is the k-th complex Fourier coefficient obtained as

$$\langle x \rangle_k(t) = \frac{1}{T}\int_{t-T}^{t} x(\tau) e^{-jk\omega_c \tau} d\tau. \tag{12}$$

This coefficient is also known as the index-k or the k-phasor [17]. As the Fourier coefficient $\langle x \rangle_k(t)$ varies with time, it receives the name of DPh [4]. The following two noteworthy properties are used in the DPh-based modeling technique:

(*i*) Differentiation of the k-th Fourier coefficient with respect to time

$$\frac{d}{dt}\langle x \rangle_k(t) = \left\langle \frac{d}{dt}x \right\rangle_k (t) - jk\omega_c \langle x \rangle_k(t). \tag{13}$$

(*ii*) Index-k average of the product of two signals $x(t)$ and $u(t)$ (convolution property)

$$\langle ux \rangle_k(t) = \sum_{\ell=-\infty}^{\infty} \langle u \rangle_{k-\ell}(t) \langle x \rangle_\ell(t). \tag{14}$$

The differentiation property can be applied to a general state-space model $\dot{x}(t) = f(x(t), u(t))$, by first computing the Fourier coefficients on both sides of the expression as follows:

$$\left\langle \frac{d}{dt}x \right\rangle_k = \langle f\{x, u\} \rangle_k \tag{15}$$

and then substituting (15) in (13), which yields

$$\frac{d}{dt}\langle x \rangle_k = \langle f\{x, u\} \rangle_k - jk\omega_c \langle x \rangle_k. \tag{16}$$

To simplify the notation, in (15), (16), and in what follows, the time argument is dropped out.

Assuming that the signals x and u are well approximated by the sum of their index-0 (DC) and the index-1 (fundamental) averages, the fundamental Fourier coefficient of such signals are given by

$$\langle x \rangle_1 = \langle x \rangle_1^{\Re} + j\langle x \rangle_1^{I}, \tag{17}$$

$$\langle u \rangle_1 = \langle u \rangle_1^{\Re} + j\langle u \rangle_1^{I}, \tag{18}$$

where $\Re$ and I indicated the coefficient's real and imaginary parts. Then, using the fact that the positive and negative indexes are complex conjugates of each other, i.e., $\langle x \rangle_1^{\Re} = \langle x \rangle_{-1}^{\Re}$, $\langle x \rangle_1^{I} = -\langle x \rangle_{-1}^{I}$, $\langle u \rangle_1^{\Re} = \langle u \rangle_{-1}^{\Re}$, $\langle u \rangle_1^{I} = -\langle u \rangle_{-1}^{I}$, the following expressions can be obtained after the application of the convolution property (14) with $\ell \in \{-1, 0, 1\}$, that is,

$$\langle ux \rangle_0 = \langle u \rangle_0 \langle x \rangle_0 + 2\left(\langle u \rangle_1^{\Re} \langle x \rangle_1^{\Re} + \langle u \rangle_1^{I} \langle x \rangle_1^{I}\right), \tag{19}$$

$$\langle ux \rangle_1^{\Re} = \langle u \rangle_0 \langle x \rangle_1^{\Re} + \langle x \rangle_0 \langle u \rangle_1^{\Re}, \tag{20}$$

$$\langle ux \rangle_1^{I} = \langle u \rangle_0 \langle x \rangle_1^{I} + \langle x \rangle_0 \langle u \rangle_1^{I}. \tag{21}$$

Expressions (16)-(21) are the basis to develop the DPhMs involving the index-0 and index-1 averages.

IV. The DPhM of the MMC

In this section, a DPhM of the MMC, comprising three cells on each arm, is developed. To obtain the index-0 model of this particular MMC, (16) and (19) are applied to the MMC model given in (1)-(4), with $n = 3$. This yields the following equations:

$$\begin{aligned}\frac{d\langle i_P\rangle_0}{dt} = \frac{1}{L}\Big(&-R\langle i_P\rangle_0 + R\langle i_N\rangle_0 - \langle u_1\rangle_0\langle v_1\rangle_0 - \langle u_2\rangle_0\langle v_2\rangle_0 \\ &- \langle u_3\rangle_0\langle v_3\rangle_0 - 2\langle u_1\rangle_1^{\Re}\langle v_1\rangle_1^{\Re} - 2\langle u_1\rangle_1^{I}\langle v_1\rangle_1^{I} \\ &- 2\langle u_2\rangle_1^{\Re}\langle v_2\rangle_1^{\Re} - 2\langle u_2\rangle_1^{I}\langle v_2\rangle_1^{I} - 2\langle u_3\rangle_1^{\Re}\langle v_3\rangle_1^{\Re} \\ &-2\langle u_3\rangle_1^{I}\langle v_3\rangle_1^{I} + \frac{E}{2}\Big),\end{aligned} \tag{22}$$

$$\begin{aligned}\frac{d\langle i_N\rangle_0}{dt} = \frac{1}{L}\Big(&R\langle i_P\rangle_0 - R\langle i_N\rangle_0 - \langle u_4\rangle_0\langle v_4\rangle_0 - \langle u_5\rangle_0\langle v_5\rangle_0 \\ &- \langle u_6\rangle_0\langle v_6\rangle_0 - 2\langle u_4\rangle_1^{\Re}\langle v_4\rangle_1^{\Re} - 2\langle u_4\rangle_1^{I}\langle v_4\rangle_1^{I} \\ &- 2\langle u_5\rangle_1^{\Re}\langle v_5\rangle_1^{\Re} - 2\langle u_5\rangle_1^{I}\langle v_5\rangle_1^{I} - 2\langle u_6\rangle_1^{\Re}\langle v_6\rangle_1^{\Re} \\ &-2\langle u_6\rangle_1^{I}\langle v_6\rangle_1^{I} + \frac{E}{2}\Big),\end{aligned} \tag{23}$$

$$\begin{aligned}\frac{d\langle v_i\rangle_0}{dt} = \frac{1}{C}\Big(&\langle u_i\rangle_0\langle i_P\rangle_0 + 2\langle u_i\rangle_1^{\Re}\langle i_P\rangle_1^{\Re} + 2\langle u_i\rangle_1^{I}\langle i_P\rangle_1^{I}\Big), \\ &\text{for} \quad i = \{1,2,3\},\end{aligned} \tag{24}$$

$$\begin{aligned}\frac{d\langle v_i\rangle_0}{dt} = \frac{1}{C}\Big(&\langle u_i\rangle_0\langle i_N\rangle_0 + 2\langle u_i\rangle_1^{\Re}\langle i_N\rangle_1^{\Re} + 2\langle u_i\rangle_1^{I}\langle i_N\rangle_1^{I}\Big), \\ &\text{for} \quad i = \{4,5,6\}.\end{aligned} \tag{25}$$

In 22 and 23, the AC voltage $v_0 = R(i_P - i_N)$ has been used, assuming that Z_0 is a resistive R load. Notice also that (24) and (25) are repeated three times each one. Therefore, the index-0 model of the MMC with $n = 3$ comprises eight equations in total, one for each cell capacitor voltage, and one for each arm current.

To obtain the MMC index-1 model, first (16) with $k = 1$ is applied to (1)-(4) ($n = 3$) and then each term $\langle\cdot\rangle$ is split in its real and imaginary parts. Next, (20) and (21) are applied to each of these expressions. Finally, the real and imaginary terms on each equation are taken apart to produce two expressions, namely the index-1 real part and the index-1 imaginary part of every equation. Application of this procedure yields the following equations:

$$\begin{aligned}\frac{d\langle i_P\rangle_1^{\Re}}{dt} = \frac{1}{L}\Big(&-\langle u_1\rangle_1^{\Re}\langle v_1\rangle_0 - \langle u_2\rangle_1^{\Re}\langle v_2\rangle_0 - \langle u_3\rangle_1^{\Re}\langle v_3\rangle_0 \\ &- R\langle i_P\rangle_1^{\Re}\Big) + \omega_c\langle i_P\rangle_1^{I} + \frac{1}{L}\Big(R\langle i_N\rangle_1^{\Re} - \langle u_1\rangle_0\langle v_1\rangle_1^{\Re} \\ &- \langle u_2\rangle_0\langle v_2\rangle_1^{\Re} - \langle u_3\rangle_0\langle v_3\rangle_1^{\Re}\Big),\end{aligned} \tag{26}$$

$$\begin{aligned}\frac{d\langle i_P\rangle_1^{I}}{dt} = \frac{1}{L}\Big(&-\langle u_1\rangle_1^{I}\langle v_1\rangle_0 - \langle u_2\rangle_1^{I}\langle v_2\rangle_0 - \langle u_3\rangle_1^{I}\langle v_3\rangle_0\Big) \\ &- \omega_c\langle i_P\rangle_1^{\Re} + \frac{1}{L}\Big(-R\langle i_P\rangle_1^{I} + R\langle i_N\rangle_1^{I} - \langle u_1\rangle_0\langle v_1\rangle_1^{I} \\ &- \langle u_2\rangle_0\langle v_2\rangle_1^{I} - \langle u_3\rangle_0\langle v_3\rangle_1^{I}\Big),\end{aligned} \tag{27}$$

$$\begin{aligned}\frac{d\langle i_N\rangle_1^{\Re}}{dt} = \frac{1}{L}\Big(&-\langle u_4\rangle_1^{\Re}\langle v_4\rangle_0 - \langle u_5\rangle_1^{\Re}\langle v_5\rangle_0 - \langle u_6\rangle_1^{\Re}\langle v_6\rangle_0 \\ &+ R\langle i_P\rangle_1^{\Re} - R\langle i_N\rangle_1^{\Re}\Big) + \omega_c\langle i_N\rangle_1^{I} \\ &+ \frac{1}{L}\Big(-\langle u_4\rangle_0\langle v_4\rangle_1^{\Re} - \langle u_5\rangle_0\langle v_5\rangle_1^{\Re} - \langle u_6\rangle_0\langle v_6\rangle_1^{\Re}\Big),\end{aligned} \tag{28}$$

$$\begin{aligned}\frac{d\langle i_N\rangle_1^{I}}{dt} = \frac{1}{L}\Big(&-\langle u_4\rangle_1^{I}\langle v_4\rangle_0 - \langle u_5\rangle_1^{I}\langle v_5\rangle_0 - \langle u_6\rangle_1^{I}\langle v_6\rangle_0 \\ &+ R\langle i_P\rangle_1^{I}\Big) - \omega_c\langle i_N\rangle_1^{\Re} + \frac{1}{L}\Big(-R\langle i_N\rangle_1^{I} - \langle u_4\rangle_0\langle v_4\rangle_1^{I} \\ &- \langle u_5\rangle_0\langle v_5\rangle_1^{I} - \langle u_6\rangle_0\langle v_6\rangle_1^{I}\Big),\end{aligned} \tag{29}$$

$$\begin{aligned}\frac{d\langle v_i\rangle_1^{\Re}}{dt} = \frac{1}{C}\Big(&\langle u_i\rangle_1^{\Re}\langle i_P\rangle_0 + \langle u_i\rangle_0\langle i_P\rangle_1^{\Re}\Big) + \omega_c\langle v_i\rangle_1^{I}, \\ &\text{for} \quad i = \{1,2,3\},\end{aligned} \tag{30}$$

$$\begin{aligned}\frac{d\langle v_i\rangle_1^{I}}{dt} = \frac{1}{C}\Big(&\langle u_i\rangle_1^{I}\langle i_P\rangle_0 + \langle u_i\rangle_0\langle i_P\rangle_1^{I}\Big) - \omega_c\langle v_i\rangle_1^{\Re}, \\ &\text{for} \quad i = \{1,2,3\},\end{aligned} \tag{31}$$

$$\begin{aligned}\frac{d\langle v_i\rangle_1^{\Re}}{dt} = \frac{1}{C}\Big(&\langle u_i\rangle_1^{\Re}\langle i_N\rangle_0 + \langle u_i\rangle_0\langle i_N\rangle_1^{\Re}\Big) + \omega_c\langle v_i\rangle_1^{I}, \\ &\text{for} \quad i = \{4,5,6\},\end{aligned} \tag{32}$$

$$\begin{aligned}\frac{d\langle v_i\rangle_1^{I}}{dt} = \frac{1}{C}\Big(&\langle u_i\rangle_1^{I}\langle i_N\rangle_0 + \langle u_i\rangle_0\langle i_N\rangle_1^{I}\Big) - \omega_c\langle v_i\rangle_1^{\Re}, \\ &\text{for} \quad i = \{4,5,6\}.\end{aligned} \tag{33}$$

As in the index-0 model, (30)-(33) are repeated three times each. Thus, the MMC index-1 model comprises 16 equations in total; a real and an imaginary set of eight equations, one for each cell capacitor voltage, and one for each arm current. The index-0 and index-1 averages of u_i are computed as indicated in [20] to take into account the phase-shift of the carriers, which yields

$$\langle u_i\rangle_0 = D_i, \qquad \forall i \in \{1,\ldots,2n\}, \tag{34}$$

$$\langle u_i\rangle_1 = \frac{1}{\pi}\sin(D_i\pi)\, e^{j\phi_i}, \quad \forall i \in \{1,\ldots,2n\}, \tag{35}$$

where D_i is the duty cycle of the i-th cell and ϕ_i is the carrier's phase for the i-th cell. Gathering the index-0 and index-1 models in a single system, results into the 24th $(3(2n+2))$ order DPhM of the MMC with $n = 3$ cells per arm, described in (36)-(43):

$$\frac{d}{dt}\mathbf{x} = \mathbf{A}\mathbf{x} + \mathbf{B}E, \tag{36}$$

with

$$\begin{aligned}\mathbf{x} = \Big[&\langle i_P\rangle_0, \langle i_N\rangle_0, \langle v_1\rangle_0, \cdots, \langle v_6\rangle_0\langle, i_P\rangle_1^{\Re}, \langle i_P\rangle_1^{I}, \langle i_N\rangle_1^{\Re}, \\ &\langle i_N\rangle_1^{I}, \langle v_1\rangle_1^{\Re}, \langle v_1\rangle_1^{I}, \cdots, \langle v_6\rangle_1^{\Re}, \langle v_6\rangle_1^{I}\Big]^{\top},\end{aligned} \tag{37}$$

$$\mathbf{A} = \left[\begin{array}{c|c} \mathbf{A}_1 & \mathbf{A}_2 \\ \hline \mathbf{A}_3 & \mathbf{A}_4 \end{array}\right], \tag{38}$$

$$\mathbf{A}_1 = \begin{bmatrix} \frac{-R}{L} & \frac{R}{L} & \frac{-\langle u_1\rangle_0}{L} & \frac{-\langle u_2\rangle_0}{L} & \frac{-\langle u_3\rangle_0}{L} & 0 & 0 & 0 & 0 & 0 & 0 & 0 \\ \frac{R}{L} & \frac{-R}{L} & 0 & 0 & 0 & \frac{-\langle u_4\rangle_0}{L} & \frac{-\langle u_5\rangle_0}{L} & \frac{-\langle u_6\rangle_0}{L} & 0 & 0 & 0 & 0 \\ \frac{\langle u_1\rangle_0}{C} & 0 & 0 & 0 & 0 & 0 & 0 & 0 & \frac{2\langle u_1\rangle_1^{\Re}}{C} & \frac{2\langle u_1\rangle_1^{I}}{C} & 0 & 0 \\ \frac{\langle u_2\rangle_0}{C} & 0 & 0 & 0 & 0 & 0 & 0 & 0 & \frac{2\langle u_2\rangle_1^{\Re}}{C} & \frac{2\langle u_2\rangle_1^{I}}{C} & 0 & 0 \\ \frac{\langle u_3\rangle_0}{C} & 0 & 0 & 0 & 0 & 0 & 0 & 0 & \frac{2\langle u_3\rangle_1^{\Re}}{C} & \frac{2\langle u_3\rangle_1^{I}}{C} & 0 & 0 \\ 0 & \frac{\langle u_4\rangle_0}{C} & 0 & 0 & 0 & 0 & 0 & 0 & 0 & 0 & \frac{2\langle u_4\rangle_1^{\Re}}{C} & \frac{2\langle u_4\rangle_1^{I}}{C} \\ 0 & \frac{\langle u_5\rangle_0}{C} & 0 & 0 & 0 & 0 & 0 & 0 & 0 & 0 & \frac{2\langle u_5\rangle_1^{\Re}}{C} & \frac{2\langle u_5\rangle_1^{I}}{C} \\ 0 & \frac{\langle u_6\rangle_0}{C} & 0 & 0 & 0 & 0 & 0 & 0 & 0 & 0 & \frac{2\langle u_6\rangle_1^{\Re}}{C} & \frac{2\langle u_6\rangle_1^{I}}{C} \\ 0 & 0 & \frac{-\langle u_1\rangle_1^{\Re}}{L} & \frac{-\langle u_2\rangle_1^{\Re}}{L} & \frac{-\langle u_3\rangle_1^{\Re}}{L} & 0 & 0 & 0 & \frac{-R}{L} & \omega_c & \frac{R}{L} & 0 \\ 0 & 0 & \frac{-\langle u_1\rangle_1^{I}}{L} & \frac{-\langle u_2\rangle_1^{I}}{L} & \frac{-\langle u_3\rangle_1^{I}}{L} & 0 & 0 & 0 & -\omega_c & \frac{-R}{L} & 0 & \frac{R}{L} \\ 0 & 0 & 0 & 0 & 0 & \frac{-\langle u_4\rangle_1^{\Re}}{L} & \frac{-\langle u_5\rangle_1^{\Re}}{L} & \frac{-\langle u_6\rangle_1^{\Re}}{L} & \frac{R}{L} & 0 & \frac{-R}{L} & \omega_c \\ 0 & 0 & 0 & 0 & 0 & \frac{-\langle u_4\rangle_1^{I}}{L} & \frac{-\langle u_5\rangle_1^{I}}{L} & \frac{-\langle u_6\rangle_1^{I}}{L} & 0 & \frac{R}{L} & -\omega_c & \frac{-R}{L} \end{bmatrix} \tag{39}$$

$$\mathbf{A}_2 = \begin{bmatrix} \frac{-2\langle u_1\rangle_1^{\Re}}{L} & \frac{-2\langle u_1\rangle_1^{I}}{L} & \frac{-2\langle u_2\rangle_1^{\Re}}{L} & \frac{-2\langle u_2\rangle_1^{I}}{L} & \frac{-2\langle u_3\rangle_1^{\Re}}{L} & \frac{-2\langle u_3\rangle_1^{I}}{L} & 0 & 0 & 0 & 0 & 0 & 0 \\ 0 & 0 & 0 & 0 & 0 & 0 & \frac{-2\langle u_4\rangle_1^{\Re}}{L} & \frac{-2\langle u_4\rangle_1^{I}}{L} & \frac{-2\langle u_5\rangle_1^{\Re}}{L} & \frac{-2\langle u_5\rangle_1^{I}}{L} & \frac{-2\langle u_6\rangle_1^{\Re}}{L} & \frac{-2\langle u_6\rangle_1^{I}}{L} \\ & & & & & \mathbf{0}_{6\times 12} & & & & & & \\ \frac{-\langle u_1\rangle_0}{L} & 0 & \frac{-\langle u_2\rangle_0}{L} & 0 & \frac{-\langle u_3\rangle_0}{L} & 0 & 0 & 0 & 0 & 0 & 0 & 0 \\ 0 & \frac{-\langle u_1\rangle_0}{L} & 0 & \frac{-\langle u_2\rangle_0}{L} & 0 & \frac{-\langle u_3\rangle_0}{L} & 0 & 0 & 0 & 0 & 0 & 0 \\ 0 & 0 & 0 & 0 & 0 & 0 & \frac{-\langle u_4\rangle_0}{L} & 0 & \frac{-\langle u_5\rangle_0}{L} & 0 & \frac{-\langle u_6\rangle_0}{L} & 0 \\ 0 & 0 & 0 & 0 & 0 & 0 & 0 & \frac{-\langle u_4\rangle_0}{L} & 0 & \frac{-\langle u_5\rangle_0}{L} & 0 & \frac{-\langle u_6\rangle_0}{L} \end{bmatrix} \tag{40}$$

$$\mathbf{A}_3 = \begin{bmatrix} \frac{\langle u_1\rangle_1^{\Re}}{C} & 0 & & \frac{\langle u_1\rangle_0}{C} & 0 & 0 & 0 \\ \frac{\langle u_1\rangle_1^{I}}{C} & 0 & & 0 & \frac{\langle u_1\rangle_0}{C} & 0 & 0 \\ \frac{\langle u_2\rangle_1^{\Re}}{C} & 0 & & \frac{\langle u_2\rangle_0}{C} & 0 & 0 & 0 \\ \frac{\langle u_2\rangle_1^{I}}{C} & 0 & & 0 & \frac{\langle u_2\rangle_0}{C} & 0 & 0 \\ \frac{\langle u_3\rangle_1^{\Re}}{C} & 0 & & \frac{\langle u_3\rangle_0}{C} & 0 & 0 & 0 \\ \frac{\langle u_3\rangle_1^{I}}{C} & 0 & \mathbf{0}_{12\times 6} & 0 & \frac{\langle u_3\rangle_0}{C} & 0 & 0 \\ 0 & \frac{\langle u_4\rangle_1^{\Re}}{C} & & 0 & 0 & \frac{\langle u_4\rangle_0}{C} & 0 \\ 0 & \frac{\langle u_4\rangle_1^{I}}{C} & & 0 & 0 & 0 & \frac{\langle u_4\rangle_0}{C} \\ 0 & \frac{\langle u_5\rangle_1^{\Re}}{C} & & 0 & 0 & \frac{\langle u_5\rangle_0}{C} & 0 \\ 0 & \frac{\langle u_5\rangle_1^{I}}{C} & & 0 & 0 & 0 & \frac{\langle u_5\rangle_0}{C} \\ 0 & \frac{\langle u_6\rangle_1^{\Re}}{C} & & 0 & 0 & \frac{\langle u_6\rangle_0}{C} & 0 \\ 0 & \frac{\langle u_6\rangle_1^{I}}{C} & & 0 & 0 & 0 & \frac{\langle u_6\rangle_0}{C} \end{bmatrix} \tag{41}$$

$$\mathbf{A}_4 = \begin{bmatrix} 0 & \omega_c & 0 & 0 & 0 & 0 & 0 & 0 & 0 & 0 & 0 & 0 \\ -\omega_c & 0 & 0 & 0 & 0 & 0 & 0 & 0 & 0 & 0 & 0 & 0 \\ 0 & 0 & 0 & \omega_c & 0 & 0 & 0 & 0 & 0 & 0 & 0 & 0 \\ 0 & 0 & -\omega_c & 0 & 0 & 0 & 0 & 0 & 0 & 0 & 0 & 0 \\ 0 & 0 & 0 & 0 & 0 & \omega_c & 0 & 0 & 0 & 0 & 0 & 0 \\ 0 & 0 & 0 & 0 & -\omega_c & 0 & 0 & 0 & 0 & 0 & 0 & 0 \\ 0 & 0 & 0 & 0 & 0 & 0 & 0 & \omega_c & 0 & 0 & 0 & 0 \\ 0 & 0 & 0 & 0 & 0 & 0 & -\omega_c & 0 & 0 & 0 & 0 & 0 \\ 0 & 0 & 0 & 0 & 0 & 0 & 0 & 0 & 0 & \omega_c & 0 & 0 \\ 0 & 0 & 0 & 0 & 0 & 0 & 0 & 0 & -\omega_c & 0 & 0 & 0 \\ 0 & 0 & 0 & 0 & 0 & 0 & 0 & 0 & 0 & 0 & 0 & \omega_c \\ 0 & 0 & 0 & 0 & 0 & 0 & 0 & 0 & 0 & 0 & -\omega_c & 0 \end{bmatrix}, \tag{42}$$

and

$$\mathbf{B} = \left[\frac{1}{2L}, \frac{1}{2L}, \mathbf{0}_{1\times 22}\right]^{\top}. \tag{43}$$

V. RESULTS

The proposed DPhM (36)-(43) of the MMC, as well as a switched version of the converter, were simulated and implemented in a real-time simulation (RTS) platform, re-

spectively, and their time responses were compared. Both implementations considered the single-phase MMC shown in Fig. 1, with n=3, and with the following parameter values: a DC-link voltage of E=420 V, a capacitance of C=3.2 mF (same for every cell), an inductance of L=1 mH (same for each arm), and a load resistance of R=16 Ω. For the PSC-PWM, the modulation index was fixed to m_a=0.9. There were two modulating signals with a fundamental frequency of f_0=50 Hz. The frequency of the triangular carrier waveforms was set to f_c=2,500 Hz. Each arm comprises three cells; hence, three triangular carriers were required per arm, i.e., one per cell. The three triangular carriers required phase-shifts of $\phi=[0, 2\pi/3, 4\pi/3]^\top$ rad. Moreover, the same set of three carriers was used in both arms, as the number of cells on each arm was odd. In what follows, we simply used Simulink/MATLAB® for the implementation of the proposed DPhM and an RTS platform for the implementation of the switched MMC.

To have a better comparison between the time responses obtained from the DPhM and the time responses from the RTS, the DPhM (36)-(43) was sampled at f_s=50 kHz. Although the DPhM can run at lower sampling frequencies, f_s was set to 50 kHz to match the scope's data recording rate for the RTS waveforms. The expressions for the switching signals, found with (34) and (35), are as follows[1]:

$$\langle u_i\rangle_0 = D_P, \quad \text{for} \quad i=\{1,2,3\},$$
$$\langle u_i\rangle_0 = D_N, \quad \text{for} \quad i=\{4,5,6\},$$

$$\begin{aligned}\langle u_1\rangle_1 &= \tfrac{1}{\pi}D_P e^{j0}, & \langle u_2\rangle_1 &= \tfrac{1}{\pi}D_P e^{j2\pi/3},\\ \langle u_3\rangle_1 &= \tfrac{1}{\pi}D_P e^{j4\pi/3}, & \langle u_4\rangle_1 &= \tfrac{1}{\pi}D_N e^{j0},\\ \langle u_5\rangle_1 &= \tfrac{1}{\pi}D_N e^{j2\pi/3}, & \langle u_6\rangle_1 &= \tfrac{1}{\pi}D_N e^{j4\pi/3},\end{aligned}$$

where D_P and D_N are given in (5) and (6), respectively.

The simulation of the proposed DPhM consists of a single Simulink file running at a sampling frequency of f_s=50 kHz. Fig. 3 shows a block diagram of the DPhM simulation. This program file contains a single MATLAB function, where the MMC parameters, DPhM, and Fourier synthesis of each MMC state variable are coded. The inputs to the MATLAB function are the time t, modulating signals D_P and D_N, and the $\mathbf{x}$ vector. The outputs from the MATLAB function are the time derivatives of the $\mathbf{x}$ vector, which are integrated to yield the $\mathbf{x}$ vector, and the waveforms of each MMC state variable obtained via the the sum of the index-0 plus the index-1 DPhM.

In the experimental RTS implementation, the single-phase MMC was emulated in a field-programmable gate array (FPGA) XC6SLX16 on the Xilinx Nexys 3 board operating at a sampling frequency of 25 MHz, and the PSC-PWM scheme was implemented in a DSP TMS320F28335 from Texas Instruments operating at a sampling frequency of f_s=15 kHz. The latter corresponds to the output effective switching frequency of the MMC. Recall that the converter comprises six cells on its phase, each switching at f_c=2.5 kHz, which leads to an effective switching frequency of 15 kHz. If the DSP allows higher sampling frequencies, then it is recommended to use integer multiples of the effective switching frequency.

[1]Simulations showed that the use of (35) generated capacitor voltages that oscillated as low frequency sinusoidal waveforms. However, avoiding the sine function, while keeping only the duty cycle, conducted to the results included in this paper.

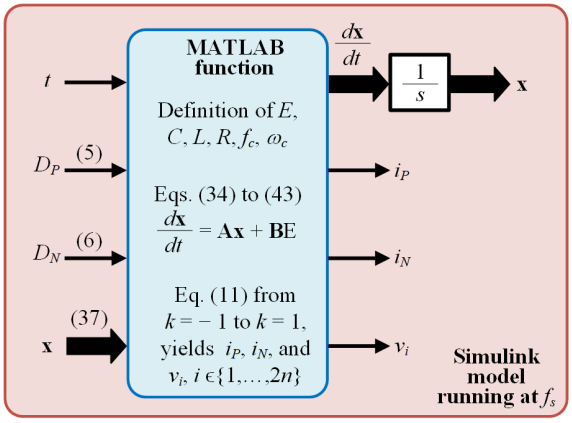

Fig. 3. Block diagram of the DPhM simulation in Simulink.

The MMC model implementation in FPGA was realized as follows: (i) expressions (1)-(4) were discretized using the forward Euler's rectangular rule [21], and (ii) the hardware description of the discretized equations was coded in VHDL using 32-bit fixed-point words to represent all variables and constants. The MMC model implementation in FPGA has also been used in other similar works [9] and [22]. It is worth to notice that responses obtained with the forward Euler's discretized MMC model and those obtained with the continuous-time MMC model are very similar as long as the sampling time is 10 μs or less [23]. In this work, we use a sampling time of 40 ns in the FPGA, thus fulfilling the guidelines given in [23] for discrete MMC models to approach the behavior of the continuous version.

In both simulation and RTS, the comparison test consisted in operating the MMC with the PSC-PWM, while imposing different initial conditions on the capacitor voltages. This has the purpose of demonstrating that, despite different initial conditions on the capacitor voltages, the PSC-PWM scheme, by itself, leads the voltages to the same average value in steady state. For the upper arm, the initial capacitor voltages were fixed to v_1=140 V, v_2=180 V and v_3=110 V, while for the lower arm, the initial capacitor voltages were fixed to v_4=160 V, v_5=140 V, and v_6=100 V.

Figs. 4(a) and 4(b) show the startup responses of the capacitor voltages on the upper and lower arms of the MMC, obtained with the the sum of the index-0 plus the index-1 models in (11), coded in Simulink. The DPhM shows that all capacitor voltages get overlapped after 12 seconds, approximately. Fig. 5(a) shows the startup responses of the capacitor voltages v_1, v_2 and v_3, while Fig. 5(b) shows the startup responses of the capacitor voltages v_4, v_5 and v_6. Figs. 5(a) and 5(b) were obtained from the RTS platform and show that the shapes of all capacitor voltages overlap after a relatively short transient. As observed in Figs. 4 and 5, both simulation and RTS results confirm the natural balancing mechanism of the MMC under the PSC-PWM.

Figs. 6(a) and 6(b) show the startup responses of the arm currents i_P and i_N, respectively, which are obtained with

the index-0 plus the index-1 DPhMs coded in the MATLAB function as indicated in Fig. 3.

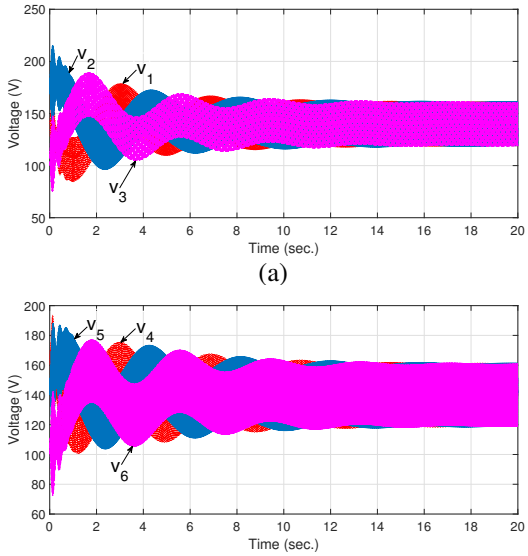

(a) (b)

Fig. 4. Capacitor voltages build with the index-0 plus the index-1 models: **(a)** v_1, v_2 and v_3 and **(b)** v_4, v_5 and v_6.

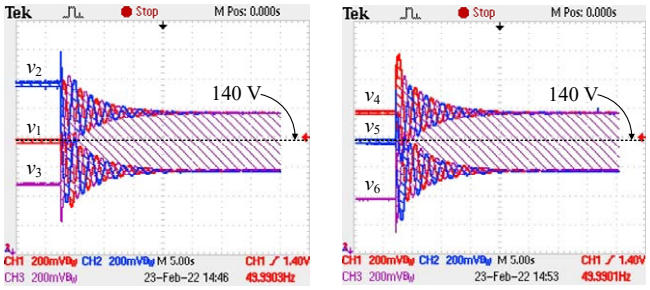

(a) (b)

Fig. 5. RTS transient responses (x-axis: 5 s/div) of the capacitor voltages on **(a)** the upper arm v_1, v_2 and v_3 (y-axis: 20.475 V/div) and **(b)** the lower arm v_4, v_5 and v_6 (y-axis: 20.475 V/div), when the initial conditions were fixed to v_1=140 V, v_2=180 V, v_3=110 V, v_4=160 V, v_5=140 V and v_6=100 V.

Figs. 7(a) and 7(b) show, for the RTS platform, the startup responses of the arm currents i_P and i_N. Both figures, 6 and 7, show that the arm currents reach the steady state in less than 2.5 seconds. Figs. 4 and 6, show that the DPhM approach may be useful to predict the transient behavior duration of the MMC state variables under the PSC-PWM scheme.

Figs. 8(a) and 8(b) show the steady-state responses of v_1 and v_4, respectively, obtained with (solid) the simulation using the index-0 plus the index-1 DPhM models, and (dotted) the switched circuit implemented in the RTS platform. Both Figs. show that the steady-state waveforms of the capacitor voltages from the DPhM simulation and those of the switched converter in the RTS are very similar to each other, even the ripple amplitude is very close. The expected steady-state average value of capacitor voltages is $E/n = 420/3 = 140$ V. The waveforms obtained with the proposed DPhM demonstrate that operating the MMC with the PSC-PWM scheme is enough to guarantee that all cell capacitor voltages will reach the expected steady-state value, thus avoiding the need to include sorting algorithms to balance the capacitor voltages.

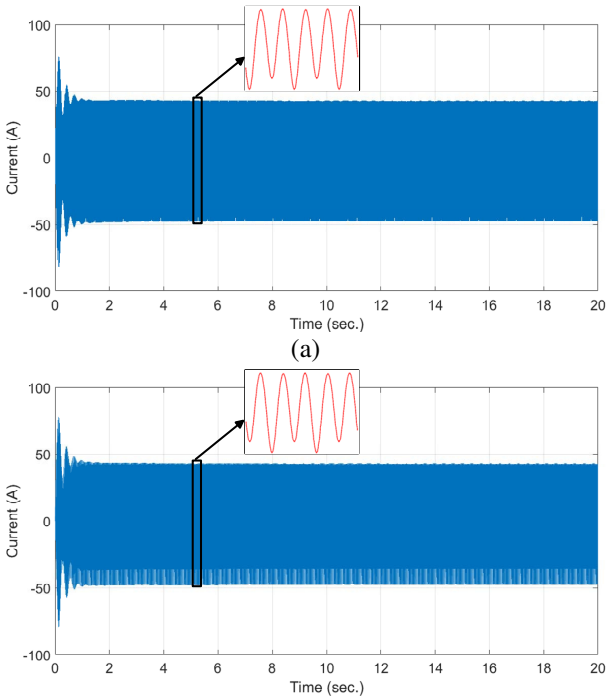

(a) (b)

Fig. 6. Arm currents obtained with the index-0 plus the index-1 of the DPhM: **(a)** i_P and **(b)** i_N.

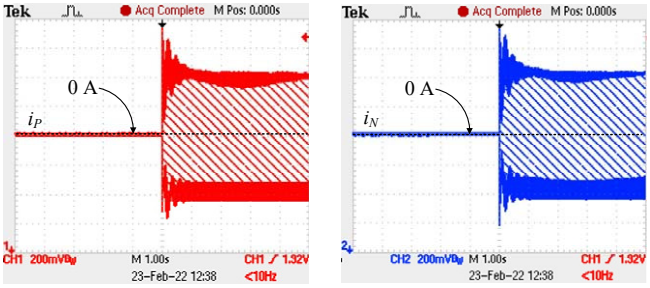

(a) (b)

Fig. 7. RTS transient responses (x-axis: 1 s/div) of the arm currents in **(a)** the upper arm i_P (y-axis: 20.475 A/div) and **(b)** the lower arm i_N (y-axis: 20.475 A/div).

Figs. 9(a) and 9(b) show the steady-state responses of the arm currents i_P and i_N, respectively, obtained with (solid) the index-0 plus the index-1 DPhM, and (dotted) the switched circuit implemented in the RTS platform. Figs. 9(a) and 9(b) show that the steady-state waveforms of the arm currents generated with the DPhM approach replicate those produced in the switching circuit implemented in the RTS platform.

Consequently, from the above results, the proposed DPhM yields comparable results to those obtained from the switched converter, helping to predict the amplitudes of all state variables in MMC under known parameters.

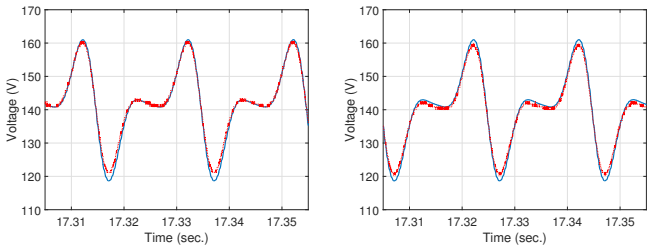

Fig. 8. Steady-state waveforms of the capacitor voltages **(a)** v_1 and **(b)** v_4 obtained with **(solid)** the DPhM simulation (comformed by index-0 plus index-1 models) and those obtained with **(dotted)** the switched circuit implemented in the RTS platform.

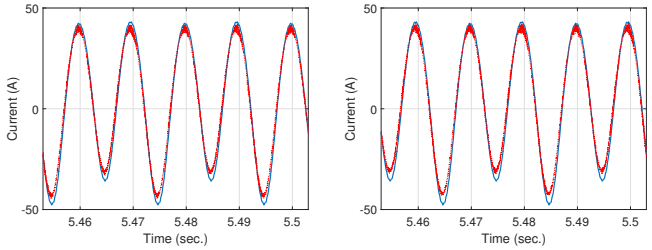

Fig. 9. Steady-state waveforms of the arm currents **(a)** i_P and **(b)** i_N obtained with the **(solid)** the DPhM simulation (composed by index-0 plus index-1 models), and those obtained with **(dotted)** the switched circuit implemented in the RTS platform.

VI. Conclusions

This paper developed a dynamic phasor-based model (DPhM) for the single-phase MMC operated with the PSC-PWM scheme, where an MMC with $n = 3$ cells on each arm was considered as a case study. The modeling process began with the state-space model of the MMC, which was then processed to find the expressions for the DC and the fundamental complex Fourier coefficients (dynamic phasors, DPh) of each original state variable. No traditional transformations (sums and differences of voltages, energy like variables, etc.) of arm variables were required in the model presented in this work. In the developed DPhM, the Fourier coefficients of the original MMC state variables became the new state variables, giving rise to a 24th-order model, as the fundamental Fourier coefficients were split into real and imaginary parts. The DPhM also involved the DPh of every switching signal on the MMC.

Performance comparisons between the DPhM and the switched MMC were carried out in Simulink/MATLAB® and in a real-time simulation (RTS) platform, respectively. For the RTS, the MMC was emulated in a field-programmable gate array, while the PSC-PWM was implemented in a digital signal processor. The test consisted in starting the MMC operation with different initial conditions on the capacitor voltages of each cell, most of them different from their steady-state value. The DPhM was able to reproduce all the waveforms of the original state variables in the MMC, even the ripple amplitude was replicated by the proposed model. Also, results showed that, after a relatively short transient, all capacitor voltages converged towards the same steady-state average value without adding an external balancing controller, i.e., by the only use of the PSC-PWM scheme. The modeling presented here can be extended to the MMC with a different number of cells on the arms by simply following the detailed guidelines provided in the case study.

References

[1] A. Lesnicar and R. Marquardt, "An Innovative Modular Multilevel Converter Topology Suitable for a Wide Power Range," in *IEEE Bologna Power Tech Conference Proceedings*, vol. 3, DOI 10.1109/PTC.2003.1304403, pp. 1–6, Bologna, Italy, Jun. 2003.

[2] P. K. Kar, A. Priyadarshi, and S. B. Karanki, "Development of an enhanced multilevel converter using an efficient fundamental switching technique," *International Journal of Electrical Power & Energy Systems*, vol. 119, DOI 10.1016/j.ijepes.2020.105960, p. 105960, 2020.

[3] S. R. Deore, P. B. Darji, and A. M. Kulkarni, "Dynamic phasor modeling of modular multi-level converters," in *IEEE 7th International Conference on Industrial and Information Systems*, DOI 10.1109/ICIInfS.2012.6304792, pp. 1–6, Chennai, India, Aug. 2012.

[4] J. Rupasinghe, S. Filizadeh, and L. Wang, "A dynamic phasor model of an MMC with extended frequency range for EMT simulations," *IEEE Journal of Emerging and Selected Topics in Power Electronics*, vol. 7, DOI 10.1109/JESTPE.2018.2886698, no. 1, pp. 30–40, Mar. 2019.

[5] O. C. Sakinci and J. Beerten, "Generalized dynamic phasor modeling of the MMC for small-signal stability analysis," *IEEE Transactions on Power Delivery*, vol. 34, DOI 10.1109/TPWRD.2019.2898468, no. 3, pp. 991–1000, Jun. 2019.

[6] O. C. Sakinci and J. Beerten, "Equivalent multiple dq-frame model of the MMC using dynamic phasor theory in the $\alpha\beta z$-frame," *IEEE Transactions on Power Delivery*, vol. 35, DOI 10.1109/TPWRD.2020.3025388, no. 6, pp. 2916–2927, Dec. 2020.

[7] A. Rashwan, M. A. Sayed, Y. Mobarak, G. Shabib, and T. Senjyu, "Predictive controller based on switching state grouping for a modular multilevel converter with reduced computational time," *IEEE Transactions on Power Delivery*, vol. 32, DOI 10.1109/TPWRD.2016.2639529, no. 5, pp. 2189–2198, Oct. 2017.

[8] S. Yang, P. Wang, and Y. Tang, "Feedback linearization-based current control strategy for modular multilevel converters," *IEEE Transactions on Power Electronics*, vol. 33, DOI 10.1109/TPEL.2017.2662062, no. 1, pp. 161–174, Jan. 2018.

[9] G. A. Catzin-Contreras, G. Escobar, A. A. Valdez-Fernandez, and M. J. Lopez-Sanchez, "A model-based controller for a single-phase grid-tied modular multilevel inverter with regulation and balance of energy," *International Transactions on Electrical Energy Systems*, vol. 29, DOI 10.1002/2050-7038.12030, no. 8, pp. 1–17, Aug. 2019.

[10] G. A. Catzin-Contreras, G. Escobar, J. E. Valdez-Resendiz, L. Ibarra, and A. A. Valdez-Fernandez, "An energy model-based controller for a three-phase grid-tied modular multilevel converter," *IEEE Access*, vol. 12, DOI 10.1109/ACCESS.2023.3343390, pp. 1130–1145, 2024.

[11] Y. Zhang, X. Pei, M. Yang, J. Li, T. Sun, H. Wang, and Y. Kang, "Multi-time scale short-circuit fault control and protection cooperative strategy for MMC-type DC distribution networks," *IEEE Journal of Emerging and Selected Topics in Power Electronics*, DOI 10.1109/jestpe.2024.3452156, pp. 1–1, 2024.

[12] T. Yang, S. Bozhko, J. Le-Peuvedic, G. Asher, and C. I. Hill, "Dynamic phasor modeling of multi-generator variable frequency electrical power systems," *IEEE Transactions on Power Systems*, vol. 31, DOI 10.1109/TPWRS.2015.2399371, no. 1, pp. 563–571, Jan. 2016.

[13] S. R. Sanders, J. M. Noworolski, X. Z. Liu, and G. C. Verghese, "Generalized averaging method for power conversion circuits," in *21st Annual IEEE Conference on Power Electronics Specialists*, DOI 10.1109/PESC.1990.131207, pp. 333–340, San Antonio, Texas, 1990.

[14] C. Liu, A. Bose, and P. Tian, "Modeling and analysis of HVDC converter by three-phase dynamic phasor," *IEEE Transactions on Power Delivery*, vol. 29, DOI 10.1109/TPWRD.2012.2236850, no. 1, pp. 3–12, Feb. 2014.

[15] W. van der Merwe, P. Hokayem, and L. Stepanova, "Analysis of the 5-cell single phase MMC natural balancing mechanism," in *IEEE Energy Conversion Congress and Exposition*, DOI 10.1109/ECCE.2014.6953864, pp. 3416–3423, Pittsburgh, PA, USA, Sep. 2014.

[16] W. van der Merwe, P. Hokayem, and L. Stepanova, "Analysis of the N-cell single phase MMC natural balancing mechanism," *IEEE Journal of Emerging and Selected Topics in Power Electronics*, vol. 2, DOI 10.1109/JESTPE.2014.2346137, no. 4, pp. 1149–1158, Dec. 2014.
[17] V. A. Caliskan, G. C. Verghese, and A. M. Stanković, "Multi-frequency averaging of DC-DC converters," in *IEEE 5th Workshop on Computers in Power Electronics*, DOI 10.1109/CIPE.1996.612345, pp. 113–119, Portland, Oregon, Aug. 1996.
[18] W. van der Merwe, "Natural balancing of the 2-cell modular multilevel converter," *IEEE Transactions on Industry Applications*, vol. 50, DOI 10.1109/TIA.2014.2322142, no. 6, pp. 4028–4035, November/December 2014.
[19] K. Ilves, L. Harnefors, S. Norrga, and H.-P. Nee, "Analysis and operation of modular multilevel converters with phase-shifted carrier PWM," *IEEE Transactions on Power Electronics*, vol. 30, DOI 10.1109/TPEL.2014.2321049, no. 1, pp. 268–283, Jan. 2015.
[20] R. H. Wilkinson, "Natural balancing of multicell converters," Ph.D. dissertation, University of Stellenbosch, Stellenbosch, South Africa, Apr. 2004.
[21] G. F. Franklin, J. D. Powell, and M. L. Workman, *Digital Control of Dynamic Systems*, 3rd ed., ch. 3, pp. 59–60. Menlo Park, California, USA: Addison-Wesley, 1997.
[22] G. A. Catzin-Contreras, G. Escobar, A. A. Valdez-Fernandez, and M. J. Lopez-Sanchez, "A current controller for the modular multilevel converter operating under distorted grid voltage," *International Transactions on Electrical Energy Systems*, vol. 28, DOI 10.1002/etep.2524, no. 4, pp. 1–16, Apr. 2018.
[23] A. Zama, A. Benchaib, S. Bacha, D. Frey, and S. Silvant, "High dynamics control for MMC based on exact discrete-time model with experimental validation," *IEEE Transactions on Power Delivery*, vol. 33, DOI 10.1109/TPWRD.2017.2707343, no. 1, pp. 477–488, Feb. 2018.

Glendy Anyali Catzin–Contreras (M'22) received the M.Eng. degree in Renewable Energies from the School of Engineering, Autonomous University of Yucatan (UADY), Merida, Mexico, in 2014. Then, she got her Ph.D. degree in Electronics Engineering from the School of Sciences, Autonomous University of San Luis Potosi (UASLP), San Luis Potosi, Mexico, in 2018. From 2023 to early 2025, she was a Post-Doctoral Researcher at the School of Engineering and Sciences, Tecnologico de Monterrey, Monterrey, Nuevo Leon, Mexico. She is currently a full-time Professor at the Universidad Politecnica de Yucatan in Ucu, Yucatan, Mexico. Her current research interests include modeling of switched converters, the repetitive control for harmonic compensation, signal processing, and real-time simulations. Dr. Catzin-Contreras is a member of the National Research Fellows System level 1 (SNII-1), CONAHCyT, Mexico.

Gerardo Escobar (SM'08) received the Ph.D. degree in automatic control from the Signals and Systems Lab. LSS-SUPELEC, Université de Paris XI, France, in 1999. From 2008 to 2012, he was a Principal Scientist with the Power Electronics Group, ABB Switzerland Ltd., Zurich, Switzerland. He is currently a Professor-Researcher with the School of Engineering and Sciences, Tecnologico de Monterrey, Nuevo Leon, Mexico. His main research interests include modeling, analysis, and control design of power electronic systems, and their applications in renewable energy systems, power quality, grid integration, active filters, inverters, dc–dc converters, multilevel converters, batteries, electrical drives, wind power, photovoltaic systems; as well as nonlinear control design, adaptive control, repetitive control, and their applications in current control, voltage balance, grid synchronization and harmonic compensation, among others. Dr. Escobar is a member of the National Research Fellows System level 3 (SNII-3), CONAHCyT, Mexico. He was an AE for the IEEE Transactions on Industrial Electronics from 2007 to 2016. He has been an Associate Editor (AE) for the IEEE Transactions on Power Electronics since 2013.

Andrés A. Valdez-Fernández (S'05-M'08-SM'20) received the Ph.D. degree in control and dynamical systems from the Potosi Institute of Scientific and Technological Research (IPICyT), Mexico, in 2009. From 2008 to 2012, he was a full-time Professor-Researcher with the National Technological Institute of Mexico, Technological Institute of Superior Studies of Irapuato (TecNM-ITESI), Mexico. He is currently a full-time Professor-Researcher with the School of Sciences, Autonomous University of San Luis Potosi (UASLP), Mexico. His research interests include analysis, modelling, and control design and fault diagnosis of active power filters, inverters, rectifiers, renewable energy systems and e-mobility systems. Dr. Valdez-Fernández is a member of the National Research Fellows System level 2 (SNII-2), CONAHCyT, Mexico.

Manuel Jesus Lopez–Sanchez received the B.Eng. degree in electronics from the Technological Institute of Mérida, Mérida, Mexico, in 2003 and the M.Sc. degree in electronics from the National Institute of Astrophysics, Optics and Electronics, Puebla, Mexico, in 2007. In August 2008, he joined the School of Engineering, Autonomous University of Yucatan, Mérida, where he is currently a Full Professor. His main research interests include the control design of power electronic and renewable energy systems and the design of digital systems.